Interpolation Methods for SAR Backprojection at THz Frequencies

Yevhen Ivanenko, Viet T. Vu, and Mats I. Pettersson
Department of Mathematics and Natural Sciences
Blekinge Institute of Technology
371 79 Karlskrona, Sweden
{yevhen.ivanenko,viet.thuy.vu,mats.pettersson}@bth.se

***Abstract*—The paper proposes the extensions of the available linear and cubic interpolation methods for backprojecting complex SAR data into an image plane. Due to the fact that the phase of complex SAR data is very sensitive to the shift in time, the proposed interpolations include the phase control of the interpolated complex values. The proposed methods are examined with the global backprojection algorithm that is used to process SAR data at THz frequencies. In numerical examples, a two-dimensional indoor THz SAR imaging for a point target is considered, where the developed interpolation methods are compared with the nearest neighbor approach.**

***Index Terms*—Complex-valued data interpolation, THz SAR, GBP.**

I. Introduction

Synthetic aperture radar (SAR) is the remote sensing technique that is widely used in various application areas. The range of applications is broad, from the spaceborne applications that allow us to study geology and hydrology at the distance of hundreds kilometres from the Earth surface to the indoor short-distance sensing measurements with high resolution at THz frequencies [1]. THz SAR imaging is a new and an active research area, where the objective is to design THz SAR imaging systems that can be mounted on different platforms, especially flying platform. For the experimental SAR systems operating at $300\,\mathrm{GHz}$ [2]–[4] and $600\,\mathrm{GHz}$ [5], mounting them on flying platform leads to several technical issues. One of foreseen issue is that at the THz frequencies, the SAR imaging system becomes sensitive to vibrations of the flying platform [6]. In this case, signal processing algorithms that are capable to handle the motion error compensation are required.

The global backprojection algorithm (GBP) [7] is the time-domain SAR imaging algorithm that can be considered as a natural solution for THz SAR systems that are mounted on flying platform. The advantages of the GBP are the capability to handle radar signals with large fractional bandwidth and the motion error compensation [8]. The GBP algorithm includes an interpolation procedure, in which the complex value for a given range time delay is interpolated from the complex SAR data. This interpolated value is then backprojected into a defined image plane. There exist various interpolation algorithms that are used for SAR applications. In [9], an evaluation of nearest neighbor, piecewise linear, four- and six-point cubic convolution, and truncated sinc interpolators is presented with the application to SAR interferometry. The evaluation recommends four-point cubic convolution interpolator as the optimal, and also six-point cubic convolution for high-resolution applications. In [10], a combination of truncated sinc interpolator with the Hanning window has been proposed to improve the coherency in SAR interferometry, and the results have shown that there is no interpolator for SAR image resampling that is optimal for all SAR data type and quality. To the knowledge of authors, none of these interpolators, excluding the nearest neighbor, has been formulated for processing complex numbers, especially for SAR data represented by complex numbers, so-called complex SAR data in the rest of this paper.

In this paper, we propose the extended versions of linear and cubic interpolations. The developed interpolators are adopted for processing complex SAR data, as a part of the global backprojection algorithm, and compared with the nearest neighbor approach. We also investigate the effects of sampling frequency on the accuracy of THz SAR image formation.

This work was supported by ELLIIT research environment under the project Multistatic High-resolution Sensing at THz.

II. Problem Setup

Consider an indoor SAR system that performs two-dimensional imaging with respect to azimuth ξ and range ρ at THz frequencies; see Fig. 1. The THz SAR system is mounted on the flying platform, such as a quadcopter, and transmits frequency-modulated signals of the form

$$s_{\mathrm{t}}(\tau) = A_{\mathrm{t}} \mathrm{e}^{\mathrm{j}2\pi f_{\mathrm{c}}\tau + \mathrm{j}\pi \frac{B}{T_{\mathrm{p}}}\tau^2}, \quad -\frac{T_{\mathrm{p}}}{2} \leq \tau \leq \frac{T_{\mathrm{p}}}{2}, \qquad (1)$$

towards the scanned area, where τ is the range time, T_{p} the pulse duration, $B = f_{\max} - f_{\min}$ the bandwidth of the signal that depends on the minimal $f_{\min}$ and maximal $f_{\max}$ frequencies, and $f_{\mathrm{c}} = (f_{\max} + f_{\min})/2$ the center frequency. The indoor SAR system is monostatic, follows the straight path with respect to the azimuth axis (for $\rho = 0$), and assume that it receives backscattered signals at the same points where the signals have been broadcasted. The received signals are of the following form

$$s_{\mathrm{r}}(\xi, \tau) = A_{\mathrm{r}} \operatorname{rect}\left(\frac{\tau - \tau_{\mathrm{d}}}{T_{\mathrm{p}}}\right) \mathrm{e}^{\mathrm{j}2\pi f_{\mathrm{c}}(\tau-\tau_{\mathrm{d}}) + \mathrm{j}\pi \frac{B}{T_{\mathrm{p}}}(\tau-\tau_{\mathrm{d}})^2}, \quad (2)$$

where A_r is the reflectivity of the scattering object that is located in the scanned area, $\mathrm{rect}\{\cdot\}$ is the rectangular window that terminates the existence of the received signal in the given range-time frame, and τ_d is the range-time delay given by $\tau_\mathrm{d} = 2R/\mathrm{c}_0$. Here, c_0 denotes the speed of light in vacuum, and R the radar range, i.e., the distance between the SAR platform and the scattering object that can be calculated as

$$R = \sqrt{(\xi - \xi_\mathrm{s})^2 + \rho_\mathrm{s}^2}, \tag{3}$$

where $(\xi, 0)$ and $(\xi_\mathrm{s}, \rho_\mathrm{s})$ are the coordinates of the platform and the scattering object, respectively.

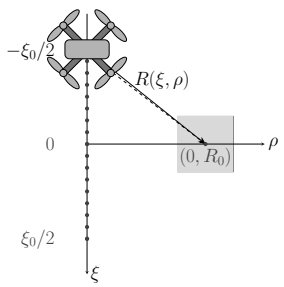

Fig. 1. Problem setup. Here, R_0 denotes the minimal range distance between the THz SAR system and the scattering object located in scanned area.

Let GBP be the imaging algorithm to be used for image formation in the THz SAR system. A SAR scene $h(\xi, \rho)$ can be reconstructed via the GBP based on the superposition of the backscattered received signals that are backprojected into a defined image plane, the slant-range plane in this problem setup. The algorithm can mathematically be expressed as

$$h(\xi, \rho) = \int_{-\xi_0/2}^{\xi_0/2} g(\xi, \tau)\, \mathrm{d}\xi. \tag{4}$$

Here, ξ_0 denotes the aperture length and $g(\xi, \tau)$ the range-compressed version of the received signal, which is obtained via the matched filtering procedure $g(\xi, \tau) = s_\mathrm{r}(\xi, \tau) * s_\mathrm{t}^*(-\tau)$, where $(\cdot)^*$ denotes the complex conjugation. The range-compressed received signal can analytically be expressed as

$$g(\xi, \tau) = \left(1 - \frac{|\tau - \tau_\mathrm{d}|}{T_\mathrm{p}}\right) \times \mathrm{sinc}\left[\pi B(\tau - \tau_\mathrm{d})\left(1 - \frac{|\tau - \tau_\mathrm{d}|}{T_\mathrm{p}}\right)\right] \mathrm{e}^{\mathrm{j}2\pi f_\mathrm{c}(\tau - \tau_\mathrm{d})}. \tag{5}$$

III. Interpolation

In this section, we briefly review several interpolation approaches for real numbers. Then we extend them to complex SAR data. Besides the nearest neighbor approach that might be applied to complex data directly, linear- and cubic-spline interpolations are also considered in this section.

A. Real-valued Data

1) Nearest Neighbor Interpolation: The nearest neighbor method is one of the simplest interpolation methods that can be described by the following relations on the interval $[x_0,\ x_1]$

$$s_\mathrm{n}(x) = \begin{cases} y_1, & \frac{1}{2}(x_1 - x_0) < x \le x_1, \\ y_0, & x_0 \le x < \frac{1}{2}(x_1 - x_0), \end{cases} \tag{6}$$

where $x_0 < x_1$. Here, y_i denotes the data value of the sample at x_i for $i = 0, 1$. The nearest neighbor interpolator (6) estimates the data s_n at the desired moment x by assigning the data value of the nearest sample as an estimated data at x.

2) Linear-spline Interpolation: The linear spline $s_\mathrm{l}(x)$ consists of a linear polynomial function on the interval $[x_0,\ x_1]$, where $x_0 < x_1$ are the knot points. The linear spline is uniquely defined by

$$s_\mathrm{l}(x) = a + b(x - x_0), \qquad x_0 \le x \le x_1 \tag{7}$$

with the corresponding derivative

$$s_\mathrm{l}'(x) = b, \qquad x_0 \le x \le x_1, \tag{8}$$

and where the polynomial coefficients $a, b \in \mathbb{R}$. The linear spline satisfies the following conditions at the knot points

$$\begin{cases} s_\mathrm{l}(x_0) = y_0, \\ s_\mathrm{l}(x_1) = y_1, \end{cases} \tag{9}$$

which imply continuity at the internal knot points, and where y_i, $i = 0, 1$, are the reference data points.

The unknown polynomial coefficients a, b can be determined by solving the system of linear equations

$$\mathbf{A}\mathbf{c} = \mathbf{y}, \tag{10}$$

which provides a unique solution and constructed based on spline conditions (9). Here,

$$\mathbf{A} = \begin{bmatrix} 1 & 0 \\ 1 & x_1 - x_0 \end{bmatrix}, \tag{11}$$

$\mathbf{c} = [a\ b]^\mathrm{T}$ and $\mathbf{y} = [y_0\ y_1]^\mathrm{T}$ are the column vectors that contain unknown coefficients and the reference data values, respectively.

3) Cubic-spline Interpolation: The cubic spline $s_\mathrm{c}(x)$ consists of piecewise cubic polynomial functions on the interval $[x_0, x_2]$, where $x_{i-1} < x_i$ for $i = 1, 2$ are the knot points. The cubic spline is uniquely defined by

$$s_{\mathrm{c},i}(x) = a_i + b_i(x - x_{i-1}) + c_i(x - x_{i-1})^2 + d_i(x - x_{i-1})^3, \qquad x_{i-1} \le x \le x_i, \tag{12}$$

on 2 subintervals with corresponding derivatives

$$s_{\mathrm{c},i}'(x) = b_i + 2c_i(x - x_{i-1}) + 3d_i(x - x_{i-1})^2, \qquad x_{i-1} \le x \le x_i, \tag{13}$$

$$s_{\mathrm{c},i}''(x) = 2c_i + 6d_i(x - x_{i-1}), \qquad x_{i-1} \le x \le x_i, \tag{14}$$

and

$$s_{\mathrm{c},i}'''(x) = 6d_i, \qquad x_{i-1} \le x \le x_i, \tag{15}$$

where the polynomial coefficients $a_i, b_i, c_i, d_i \in \mathbb{R}$. The cubic spline satisfies the following conditions at the knot points

$$\begin{cases} s_{\mathrm{c},i}(x_{i-1}) = y_{i-1}, \\ s_{\mathrm{c},i}(x_i) = y_i, \\ s_{\mathrm{c},i}'(x_i) = s_{\mathrm{c},i+1}'(x_i), \\ s_{\mathrm{c},i}''(x_i) = s_{\mathrm{c},i+1}''(x_i) \end{cases} \tag{16}$$

for $i = 1, 2$ and where the last two conditions are not applicable to the points x_0 and x_2. Here, y_i corresponds to the reference data points.

By employing the spline conditions (16), let $\delta_{i-1} = x_i - x_{i-1}$ and $s''_{\mathrm{c},i}(x_{i-1}) = p_{i-1}$ for $i = 1, 2$ such that $p_{i-1} = 2c_i$, from which the unknown polynomial coefficients a_i, b_i, c_i, and d_i of the cubic spline can be determined as

$$\begin{cases} a_i = y_{i-1}, \\ b_i = \dfrac{y_i - y_{i-1}}{\delta_{i-1}} - \dfrac{p_i + 2p_{i-1}}{6}\delta_{i-1}, \\ c_i = \dfrac{p_{i-1}}{2}, \\ d_i = \dfrac{p_i - p_{i-1}}{6\delta_{i-1}}. \end{cases} \tag{17}$$

The unknown parameters p_0, p_1, p_2 can be determined by solving a system of 3 linear equations

$$\mathbf{A}\mathbf{c} = \mathbf{y}. \tag{18}$$

However, to get a unique solution, two boundary conditions have to be applied. In this paper, we employ the natural boundary conditions at the edge knot points, i.e., $s''_{\mathrm{c},1}(x_0) = s''_{\mathrm{c},2}(x_2) = 0$. Thus, the components of (18) can be defined as

$$\mathbf{A} = \begin{bmatrix} 1 & 0 & 0 \\ \delta_0 & 2(\delta_0 + \delta_1) & \delta_1 \\ 0 & 0 & 1 \end{bmatrix}, \tag{19}$$

$$\mathbf{y} = 6 \begin{bmatrix} 0 \\ \frac{y_0}{\delta_0} - y_1\left(\frac{1}{\delta_0} + \frac{1}{\delta_1}\right) + \frac{y_2}{\delta_1} \\ 0 \end{bmatrix}, \tag{20}$$

and $\mathbf{c} = [p_0\ p_1\ p_2]^{\mathrm{T}}$. The solution to (18) can then be substituted to (17) to determine the unknown polynomial coefficients of the cubic spline.

B. Complex-valued SAR Data

Monostatic SAR systems commonly broadcast frequency-modulated signals to the scanned area and also receive echoes of a similar waveform that have been backscattered from the targets in that area. The backscattered echoes are post-processed (filtered) by SARs and the resulting range-compressed signal is of the form

$$g(\xi, \tau) \approx \mathrm{sinc}\left[\pi B(\tau - \tau_{\mathrm{d}})\right] \mathrm{e}^{\mathrm{j}2\pi f_{\mathrm{c}}(\tau - \tau_{\mathrm{d}})}, \tag{21}$$

which has a complex-valued representation in the time domain and where it is assumed that the pulse duration $T_{\mathrm{p}} \gg \tau - \tau_{\mathrm{d}}$. None of the interpolators described in Section III-A, with the exception of the nearest neighbor approach, provides an opportunity to interpolate complex numbers. In this section, we introduce the extensions of linear- and cubic-spline interpolators that are adopted for processing complex SAR data.

1) Linear-spline Interpolation: The linear spline for processing the complex SAR data $s_{\mathrm{lc}}(\tau)$ is a piecewise linear polynomial function on the interval $[\tau_0, \tau_1]$, $\tau \in \mathbb{R}$, where $\tau_0 < \tau_1$ are the knot points. The linear spline s_{lc} is uniquely defined by

$$s_{\mathrm{lc}}(\tau) = a + b(\tau - \tau_0), \qquad \tau_0 \le \tau \le \tau_1 \tag{22}$$

with the corresponding derivative

$$s'_{\mathrm{lc}}(\tau) = b, \qquad \tau_0 \le \tau \le \tau_1, \tag{23}$$

and where the polynomial coefficients $a, b \in \mathbb{C}$.

The unknown polynomial coefficients a and b can be determined by solving the system of linear equations, which can be constructed based on spline conditions. However, in comparison with the real-valued data case, additional procedures are required. Let τ_{p} denote the range time needed for a frequency-modulated signal to be transmitted from the SAR system to the given pixel of the scanned area and backwards, which can be determined as

$$\tau_{\mathrm{p}} = \frac{2}{\mathrm{c}_0}\sqrt{(\xi - \xi_{\mathrm{p}})^2 + \rho_{\mathrm{p}}^2}, \tag{24}$$

where $(\xi, 0)$ and $(\xi_{\mathrm{p}}, \rho_{\mathrm{p}})$ are the coordinates of the SAR platform and a pixel of the defined image plane, respectively. The phase of the range-compressed signal (21) is the component that contains information about the range time delay τ_{d}, which consequently corresponds to the range distance between the SAR platform and the target. Similarly, the information about the range distance between the SAR platform and the given pixel of the defined image plane can be contained in the range time parameter τ_{p}. Assume that $\tau_0 < \tau_{\mathrm{p}} < \tau_1$. To estimate the data value of sample τ_{p} accurately, a priori knowledge about the distance has to be integrated to the phase of the unknown parameter $s(\tau_{\mathrm{p}})$. This can be achieved by extending the spline conditions to the form

$$s_{\mathrm{lc}}(\tau_i) = y_i \mathrm{e}^{\mathrm{j}2\pi f_{\mathrm{c}}(\tau_{\mathrm{p}} - \tau_i)} \tag{25}$$

for $i = 0, 1$. The resulting filter function for estimation of complex-valued data value at sample τ_{p} based on linear interpolation is given by

$$s_{\mathrm{lc}}(\tau_{\mathrm{p}}) = a + b(\tau_{\mathrm{p}} - \tau_0), \tag{26}$$

where the polynomial coefficients $a = \tilde{y}_0$, and $b = (\tilde{y}_1 - \tilde{y}_0)/(\tau_1 - \tau_0)$, where $\tilde{y}_i = y_i \mathrm{e}^{\mathrm{j}2\pi f_{\mathrm{c}}(\tau_{\mathrm{p}} - \tau_i)}$ for $i = 0, 1$.

2) Cubic-spline Interpolation: The cubic spline for processing the complex SAR data $s_{\mathrm{cc}}(\tau)$ consists of piecewise cubic polynomial functions on the interval $[\tau_0, \tau_2]$, $\tau \in \mathbb{R}$, where $\tau_{i-1} < \tau_i$ for $i = 1, 2$ are the knot points. The cubic spline $s_{\mathrm{cc},i}$ is uniquely defined by

$$\begin{aligned} s_{\mathrm{cc},i}(\tau) = a_i + b_i(\tau - \tau_{i-1}) + c_i(\tau - \tau_{i-1})^2 \\ + d_i(\tau - \tau_{i-1})^3, \qquad \tau_{i-1} \le \tau \le \tau_i, \end{aligned} \tag{27}$$

on given 2 subintervals with corresponding derivatives

$$\begin{aligned} s'_{\mathrm{cc},i}(\tau) = b_i + 2c_i(\tau - \tau_{i-1}) \\ + 3d_i(\tau - \tau_{i-1})^2, \qquad \tau_{i-1} \le \tau \le \tau_i, \end{aligned} \tag{28}$$

$$s''_{\mathrm{cc},i}(\tau) = 2c_i + 6d_i(\tau - \tau_{i-1}), \qquad \tau_{i-1} \le \tau \le \tau_i, \quad (29)$$

and

$$s'''_{\mathrm{cc},i}(\tau) = 6d_i, \qquad \tau_{i-1} \le \tau \le \tau_i, \quad (30)$$

where the polynomial coefficients $a_i, b_i, c_i, d_i \in \mathbb{C}$.

Let the range time τ_{p} needed for a frequency-modulated signal to be transmitted from the SAR platform to the given pixel of the defined image plane and backwards be defined by (24), such that $\tau_0 < \tau_{\mathrm{p}} < \tau_1$. To estimate the data value of sample τ_{p} based on the cubic-spline interpolation accurately, a prior information about the phase of the unknown parameter has to be predefined and integrated to the spline conditions, resulting as

$$s_{\mathrm{cc},i}(\tau_i) = y_i \mathrm{e}^{\mathrm{j}2\pi f_{\mathrm{c}}(\tau_{\mathrm{p}} - \tau_i)} \quad (31)$$

for $i = 0, 1, 2$ and

$$s'_{\mathrm{cc},i}(\tau_i) = s'_{\mathrm{cc},i+1}(\tau_i), \quad s''_{\mathrm{cc},i}(\tau_i) = s''_{\mathrm{cc},i+1}(\tau_i) \quad (32)$$

for $i = 0, 1$. Furthermore, let $\delta_{i-1} = \tau_i - \tau_{i-1}$. By employing the spline conditions (31) and (32), let $s''_{\mathrm{cc},i}(\tau_{i-1}) = p_{i-1}$ for $i = 2$ such that $p_{i-1} = 2c_i$. The unknown parameters p_0, p_1, and p_2 can be uniquely determined by solving the following system of linear equations

$$\begin{bmatrix} 1 & 0 & 0 \\ \delta_0 & 2(\delta_0 + \delta_1) & \delta_1 \\ 0 & 0 & 1 \end{bmatrix} \begin{bmatrix} p_0 \\ p_1 \\ p_2 \end{bmatrix} = 6 \begin{bmatrix} 0 \\ \frac{\tilde{y}_0}{\delta_0} - \tilde{y}_1 \frac{\delta_0 + \delta_1}{\delta_0 \delta_1} + \frac{\tilde{y}_2}{\delta_1} \\ 0 \end{bmatrix}, \quad (33)$$

which includes the natural boundary conditions at the knot points $s''_{\mathrm{cc},1}(\tau_0) = s''_{\mathrm{cc},2}(\tau_2) = 0$. Here, $\tilde{y}_i = y_i \mathrm{e}^{\mathrm{j}2\pi f_{\mathrm{c}}(\tau_{\mathrm{p}} - \tau_i)}$ for $i = 0, 1, 2$. The resulting filter function based on cubic-spline interpolation is given by

$$s_{\mathrm{cc},1}(\tau_{\mathrm{p}}) = a_1 + b_1(\tau_{\mathrm{p}} - \tau_0) + c_1(\tau_{\mathrm{p}} - \tau_0)^2 + d_1(\tau_{\mathrm{p}} - \tau_0)^3, \quad (34)$$

where the complex-valued polynomial coefficients are $a_1 = \tilde{y}_0$, $b_1 = (\tilde{y}_1 - \tilde{y}_0)/\delta_0 - (p_1 + 2p_0)/6$, $c_1 = p_0/2$, and $d_1 = (p_1 - p_0)/6h_0$.

IV. Numerical Examples

In this section, we present some simulations, where the interpolation techniques introduced in Section III-B are incorporated with the GBP. The proposed methods are compared with the nearest neighbor approach. As a case study, we consider a two-dimensional indoor THz SAR imaging for a point target. Assume that a point target is in the center of SAR scene and that the minimal range distance between the imaging system and the target is $R_0 = 0.12\,\mathrm{m}$. Furthermore, assume that the THz SAR system has characteristics similar to the system described in [4]. The system transmits frequency-modulated signals (1) of duration $T_{\mathrm{p}} = 0.1\,\mu\mathrm{s}$ with the baseband bandwidth $[0.22,\ 0.33]\,\mathrm{THz}$ and the corresponding center frequency $f_{\mathrm{c}} = 0.275\,\mathrm{THz}$. The total number of measurements is $N_\xi = 23$, which are equidistantly performed along the azimuth ξ-axis with the step $\Delta_\xi = 0.955\,\mathrm{mm}$, such that the integration angle $\phi_0 = 10^\circ$.

Fig. 2 depicts reconstructed SAR scenes h of resolution 251×251 pixels that have been obtained with nearest neighbor (6), linear (26), and cubic interpolation (34) techniques, respectively. In Figs. 2a–c, the sampling rate is the Nyquist rate, i.e., $f_{\mathrm{s}} = 2f_{\max} = 0.66\,\mathrm{THz}$, and in Figs. 2d–f, the upsampled case with the rate $f_{\mathrm{s}} = 4f_{\max} = 1.32\,\mathrm{THz}$ is considered. Here, the intensity of SAR scenes is normalized with respect to the peak intensity for the corresponding case. Note that the SAR scenes are plotted as functions of normalized azimuth ξ_{n} and range ρ_{n}, which have been normalized with $\sin(\phi_0/2)$ and a half of the fractional bandwidth, respectively. It has been observed that for the sampling rate $f_{\mathrm{s}} = 2f_{\max}$, the SAR scene obtained with the nearest neighbor interpolation contains rough representation of the point target in comparison with the scenes, in reconstruction of which linear- and cubic-spline filters have been used. The reason of the observed phenomenon is that the nearest neighbor method assigns the nearest complex-valued data to the sample of interest and correspondingly, the phase of the estimated parameter is not in agreement with the range time τ_{p} and the range distance between the SAR system and the pixel of the defined image plane. However, when the sampling rate is increased twice, i.e., $f_{\mathrm{s}} = 4f_{\max}$, nearest neighbor interpolation provides accurate visualization of the point target; see Figs. 2d and 2a for comparison.

Fig. 3 depicts the comparison of three reconstructed SAR-scene functions $h(0, \rho_{\mathrm{n}})$ normalized with the energy contained in the $-3\,\mathrm{dB}$ main-lobe width that have been obtained with nearest neighbor, linear, and cubic interpolation methods, respectively. The SAR scenes are plotted as functions of normalized range ρ_{n}. In the case when the sampling rate $f_{\mathrm{s}} = 2f_{\max}$ that is shown in Fig. 3a, the scene function $h(0, \rho_{\mathrm{n}})$ obtained with nearest neighbor interpolation is rough and has higher intensity, which is caused by disagreement between the phase of estimated complex-valued parameter and the distance between the imaging system and the pixel of the defined image plane. The result also demonstrates that the main-lobe width of $h(0, \rho_{\mathrm{n}})$ obtained with the nearest neighbor approach is smaller than the main-lobe widths of functions obtained via linear- and cubic-spline filters (0.005 for nearest neighbor and 0.0055 for other presented methods). Hence, it can be concluded that linear- and cubic-spline interpolation methods provide more accurate results of processing complex SAR data for the Nyquist sampling rate $f_{\mathrm{s}} = 2f_{\max} = 0.66\,\mathrm{THz}$.

In Fig. 3b is shown the comparison of SAR-scene function $h(0, \rho_{\mathrm{n}})$ obtained with the nearest neighbor approach for upsampled signals at the rate $f_{\mathrm{s}} = 4f_{\max} = 1.32\,\mathrm{THz}$ with the results obtained via linear and cubic interpolations for the Nyquist rate $f_{\mathrm{s}} = 2f_{\max} = 0.66\,\mathrm{THz}$. The upsampling procedure of the range-compressed signals $g(\xi, \tau)$ was performed by zero padding of their spectra in the frequency domain by the factor of 2 and further inverse transformation to the time domain. The result demonstrates that the SAR scene obtained via the nearest neighbor approach for $f_{\mathrm{s}} = 4f_{\max}$ becomes smooth, which improves visualization of the point target as depicted in Fig. 2d, and its main lobe agrees with the main lobes of other considered functions with respect to width (0.0055) and normalized intensity. However, the

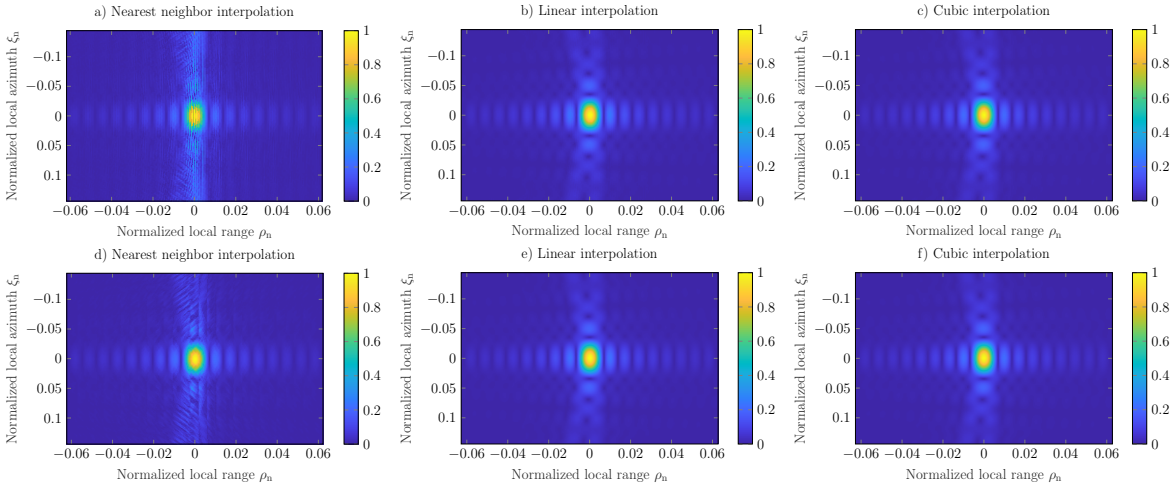

Fig. 2. Reconstructed SAR scenes h of resolution 251×251 pixels with nearest neighbor, linear, and cubic interpolations. Here, the sampling rate: a–c) $f_s = 2f_{max} = 0.66\,\text{THz}$; d–f) $f_s = 4f_{max} = 1.32\,\text{THz}$.

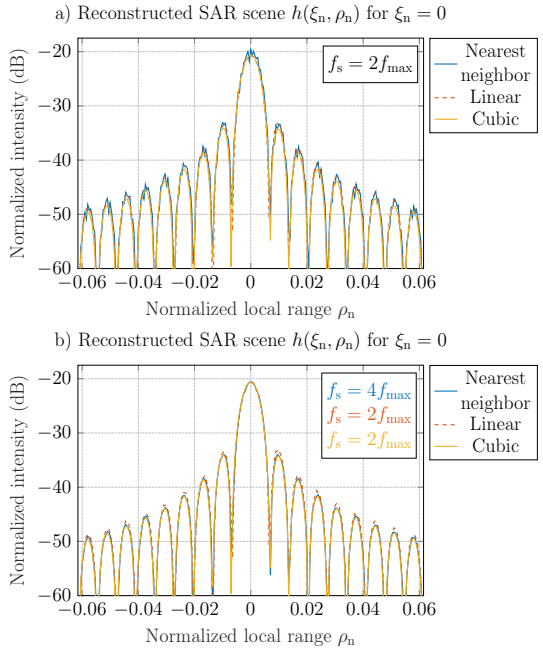

Fig. 3. Reconstructed SAR scene $h(0, \rho_n)$ at normalized azimuth $\xi_n = 0$ with nearest neighbor, linear, and cubic interpolations, respectively. Here, the sampling frequency: a) $f_s = 2f_{max} = 0.66\,\text{THz}$; b) $f_s = 4f_{max} = 1.32\,\text{THz}$ for result obtained via the nearest neighbor approach and $f_s = 2f_{max} = 0.66\,\text{THz}$ for results obtained with linear and cubic interpolations.

intensity of sidelobes of $h(0, \rho_n)$ for the upsampled case based on nearest neighbor interpolation is higher than intensity of the corresponding sidelobes of the scene obtained with cubic-spline filter for the Nyquist sampling rate. Hence, it can be concluded that cubic-spline interpolation is appropriate for THz SAR imaging process among the considered methods and provides accurate results without the upsampling procedure.

V. Conclusions

In this paper, the available linear- and cubic-spline interpolations for real numbers have been extended for complex SAR data. The developed interpolators have been incorporated with the global backprojection algorithm to process complex SAR data at THz frequencies. Through the numerical examples, it has been investigated that cubic-spline filter provides an accurate reconstruction of the SAR scene for the case when the sampling rate is the Nyquist rate, i.e., $f_s = 2f_{max}$, and thus, there is no need to perform the upsampling procedure.

References

[1] A. Batra, M. Wiemeler, D. Goehringer, and T. Kaiser, "Simulation Validation of High Resolution Indoor Terahertz Synthetic Aperture Radar Imaging," in *2020 14th European Conference on Antennas and Propagation (EuCAP)*. IEEE, 2020, pp. 1–5.

[2] M. Caris, S. Stanko, S. Palm, R. Sommer, A. Wahlen, and N. Pohl, "300 GHz Radar for High Resolution SAR and ISAR Applications," in *2015 16th International Radar Symposium (IRS)*. IEEE, 2015, pp. 577–580.

[3] Y. Zantah, F. Sheikh, A. A. Abbas, M. Alissa, and T. Kaiser, "Channel Measurements in Lecture Room Environment at 300 GHz," in *2019 Second International Workshop on Mobile Terahertz Systems (IWMTS)*. IEEE, 2019, pp. 1–5.

[4] A. Batra, V. T. Vu, Y. Zantah, M. Wiemeler, M. I. Pettersson, D. Goehringer, and T. Kaiser, "Sub-mm Resolution Indoor THz Range and SAR Imaging of Concealed Object," in *2020 IEEE MTT-S International Conference on Microwaves for Intelligent Mobility (ICMIM)*. IEEE, 2020, pp. 1–4.

[5] T. Bryllert, K. B. Cooper, R. J. Dengler, N. Llombart, G. Chattopadhyay, E. Schlecht, J. Gill, C. Lee, A. Skalare, I. Mehdi *et al.*, "A 600 GHz imaging radar for concealed objects detection," in *2009 IEEE Radar Conference*. IEEE, 2009, pp. 1–3.

[6] H. Wang, Y. Zhang, B. Wang, and J. Sun, "A novel helicopter-borne terahertz SAR imaging algorithm based on Keystone transform," in *2014 12th International Conference on Signal Processing (ICSP)*. IEEE, 2014, pp. 1958–1962.

[7] L.-E. Andersson, "On the determination of a function from spherical averages," *SIAM Journal on Mathematical Analysis*, vol. 19, no. 1, pp. 214–232, 1988.

[8] V. T. Vu and M. I. Pettersson, "Derivation of Bistatic SAR Resolution Equations Based on Backprojection," *IEEE Geoscience and Remote Sensing Letters*, vol. 15, no. 5, pp. 694–698, 2018.

[9] R. Hanssen and R. Bamler, "Evaluation of Interpolation Kernels for SAR Interferometry," *IEEE Transactions on Geoscience and Remote Sensing*, vol. 37, no. 1, pp. 318–321, 1999.

[10] Z. Li and J. Bethel, "Image coregistration in SAR interferometry," *The International Archives of the Photogrammetry, Remote Sensing and Spatial Information Sciences*, vol. 37, pp. 433–438, 2008.